Original Article

MOLECULAR METABOLISM

Three-dimensional volume fluorescence-imaging of vascular plasticity in adipose tissues

Ying Cao [1,4,6], Huanhuan Wang [5,6], Qi Wang [1,4], Xiangli Han [5], Wenwen Zeng [1,2,3,*]

ABSTRACT

Objective: The vascular system is central to sustaining tissue survival and homeostasis. Blood vessels are densely present in adipose tissues and exert essential roles in their metabolism. However, conventional immunohistochemistry methods have intrinsic limitations in examining the 3D vascular network in adipose tissues as well as other organs in general.

Methods: We established a 3D volume fluorescence-imaging technique to visualize the vasculatures in mouse adipose tissues by combining the optimized steps of whole-mount immunolabeling, tissue optical clearing, and lightsheet volume fluorescence-imaging. To demonstrate the strength of this novel imaging procedure, we comprehensively assessed the intra-adipose vasculatures under obese conditions or in response to a cold challenge.

Results: We show the entirety of the vascular network in mouse adipose tissues on the whole-tissue level at a single-capillary resolution for the first time in the field. We accurately quantify the pathological changes of vasculatures in adipose tissues in wild-type or obese mice (*ob/ob*, *db/db*, or diet-induced obesity). In addition, we identify significant and reversible changes of the intra-adipose vasculatures in the mice subjected to cold challenge (i.e., 4°). Furthermore, we demonstrate that the cold-induced vascular plasticity depends on the sympathetic-derived catecholamine signal and is involved in the beiging process of white adipose tissues.

Conclusions: We report a 3D volume fluorescence-imaging procedure that is compatible with many areas of vascular research and is poised to serve the field in future investigations of the vascular system in adipose tissues or other research scenarios.

Keywords 3D volume fluorescence-imaging; Vascular plasticity; Adipose tissues; Sympathetic arborizations; Obesity; Cold-induced beiging

1. INTRODUCTION

The vascular system sustains tissue survival, metabolism and homeostasis. Both white adipose tissues (WAT) and brown adipose tissues (BAT) are densely vascularized. Moreover, adipose tissues, particularly BAT, are among the most highly vascularized organs of the body, with each adipocyte appearing in direct contact with capillaries [1—4]. Adipose tissues are the key energy-storage depots and are also an important hormone-producing organ; they exert indispensable metabolic roles in energy homeostasis. It has been broadly recognized that dysregulation of adipose metabolism leads to obesity, type 2 diabetes and other profound metabolic diseases [5—8].

Deciphering the physiological functions of the vascular system in adipose tissues has been an area of intense research. Extensive studies have demonstrated that the local vascular system has critical involvements in the physiology and disease of adipose tissues [1,7,9—12]. Moreover, the intra-adipose vasculatures increase or decrease their density in response to various metabolic stimuli or stresses. These functional changes of the vasculatures, i.e., vascular plasticity, directly affect the local flux of oxygen, nutrients, hormones, immune cells, and other regulatory components in adipose tissues [9—12]. Furthermore, it has been increasingly appreciated that modulation of the vasculatures may exert significant and long-lasting effects on adipose metabolism, which holds promise for the therapeutic prevention and treatment of obesity, diabetes and other metabolic disorders [1,7,10—19].

However, our knowledge of the intra-adipose vascular system must be furthered. In particular, the regulatory mechanism that underlies the vascular plasticity in adipose tissues remains to be better elucidated. Notably, common experimental methods to examine the vasculatures are predominately based on bright-field or fluorescence imaging of immunohistochemistry-processed tissue sections. These conventional methods have intrinsic limitations in assessing the 3D vascular network in adipose tissues, as well as other organs in general. This

[1]Center for Life Sciences, Tsinghua University, Beijing, 100084, China [2]Institute for Immunology and School of Medicine, Tsinghua University, Beijing, 100084, China [3]Beijing Key Laboratory for Immunological Research on Chronic Diseases, Beijing, 100084, China [4]Academy for Advanced Interdisciplinary Studies, Peking University, 100871, Beijing, China [5]School of Life Sciences, Peking University, Beijing, 100871, China

[6] Authors contributed equally to this work.

*Corresponding author. Room D318, School of Medicine, Tsinghua University, Beijing, 100084, China. Tel.: +8610 62782861. E-mail: wenwenzeng@tsinghua.edu.cn (W. Zeng).

Abbreviations: WAT, white adipose tissues; BAT, brown adipose tissues; iDISCO, immunolabeling-enabled three-dimensional imaging of solvent-cleared organs; DIO, diet-induced obesity

Received May 2, 2018 • Revision received May 16, 2018 • Accepted June 2, 2018 • Available online 7 June 2018

https://doi.org/10.1016/j.molmet.2018.06.004

technical hurdle has continuously impeded the ongoing research in the field, urging our effort to develop new techniques to visualize the 3D vascular network.

Here, we report a 3D volume fluorescence-imaging procedure that has been optimized to become fully compatible with a variety of vascular research endeavors, based on the iDISCO/3DISCO technique [20,21]. With this advanced imaging power, we present for the first time in the field the entirety of the vascular network in mouse WAT and BAT at a single-capillary resolution. In addition, this 3D imaging technique has enabled the accurate quantification of vasculatures in adipose tissues. To demonstrate the unique strength of this imaging technique, we assess the pathological remodeling of vasculatures in adipose tissues under obese conditions. Furthermore, we characterize the physiological changes of vasculatures in WAT in response to a cold challenge. Moreover, we show that this cold-induced vascular plasticity depends on the sympathetic-derived catecholamine signal and is involved in the beiging process. This technical advance, together with our important findings, is poised to serve the field in future investigations of the vascular system in adipose tissues or other research scenarios.

2. MATERIAL AND METHODS

Additional information and requests for resources and reagents should be directed to and will be fulfilled by Wenwen Zeng (correspondence to wenwenzeng@tsinghua.edu.cn).

2.1. Animal information

All experimental procedures in mice were conducted in compliance with the protocol approved by the Institutional Animal Care and Use Committee (IACUC) of Tsinghua University, following the National Institutes of Health Guide for the Care and Use of Laboratory Animals.

Animals were maintained on 12-hr light/12-hr dark cycles with chow diet and water available *ad libitum*. The mice utilized in the experiments were females at the age of 8–12 weeks, with the exception of the diet-induced obesity (DIO) mice, which were at the age of 20 weeks. Wild-type C57BL/6 and DIO mice were purchased from Charles River International. *Tek-Cre* (JAX 008863, RRID:IMSR_JAX:008863), *Rosa26-LSL-tdTomato* (JAX 007914, RRID:IMSR_JAX:007914), Lep^{ob} (JAX 000632, RRID:IMSR_JAX:000632), $Lepr^{db}$ (JAX 000697, RRID:IMSR_JAX:000697), *Rosa26-LSL-EGFP* (JAX 024750, RRID:IMSR_JAX:024750), *Th-Cre* (JAX 008601, RRID:IMSR_JAX:008601), $TrkA^{fl/fl}$ (JAX 022362, RRID:IMSR_JAX:022362), $Adrb1^{-/-}$;$Adrb2^{-/-}$ (JAX 003810, RRID:IMSR_JAX:003810), and $Adrb3^{-/-}$ (JAX 006402, RRID:IMSR_JAX:006402) were obtained from the Jackson Laboratory and in-house bred to produce littermates, which were randomly assigned to experimental groups.

The strategy of generating the $Ucp1^{CreERT2/+}$ knock-in mouse line is illustrated in Fig. S3C. The targeting vector was constructed with the IRES (internal ribosome entry site) followed by the Cre^{ERT2} sequence inserted immediately after the stop codon of the *Ucp1* coding region. Linearized targeting vector was delivered together with Cas9 mRNA/sgRNA (5′-GTACCACATAAGCAACTTGGAGG-3′) into C57BL/6 mouse zygotes via microinjection. The resulting littermates were screened by PCR genotyping, DNA sequencing and Southern blot. The correctly targeted $Ucp1^{CreERT2/+}$ founders were backcrossed with C57BL/6 wild-type mice for two generations prior to being bred with the *Rosa26-LSL-EGFP* reporter mouse line.

The mice of the indicated genotypes were transferred from room temperature (22–23 °C) to 4 °C for the cold challenge or to 32 °C for the thermal-neutral condition. To induce the Cre-recombinase activity in the $Ucp1^{CreERT2/+}$; *Rosa26-LSL-EGFP* mice, 4-hydroxytamoxifen was formulated in DMSO/Kolliphor-EL/5% sucrose (1:3:6) and administered daily to the mice at 20 mg/kg of body weight via oral gavage for 4 days. The colorimetric or fluorescent dyes were administered to the mice via intravenous injection: Evans blue (Sigma, 25 mg/kg of body weight), 2,000,000 MW-Dextran Tetramethylrhodamine (Thermo Fisher Scientific #D7139, 20 mg/kg of body weight), and Isolectin GS-IB4 Alexa647 (Thermo Fisher Scientific #I32450, 2.5 mg/kg of body weight).

To pharmacologically destruct the sympathetic arborizations in inguinal WAT, the wild-type mice were anesthetized and an abdominal midline incision in the skin was made. The skin was separated to the sides to expose the inguinal WAT. 6-hydroxydopamine (Sigma, 10 μg/μl freshly prepared in 0.1% ascorbic acid) were evenly administered along each fat pad (10 μl per tissue), and the skin incision was subsequently sutured. Experiments were conducted in the mice 6 days after the treatment.

2.2. Antibodies

The primary antibodies used for immunolabeling included rat anti-CD31/PECAM-1 (BD Biosciences #553370, RRID:AB_394816), rabbit anti-RFP (Rockland #600-401-379, RRID:AB_2209751), goat anti-Perilipin (Abcam #ab61682, RRID:AB_944751), rat anti-CD11b (AbD Serotec #MCA74EL, RRID:AB_2129277), rabbit anti-Tyrosine hydroxylase (Millipore #AB152, RRID:AB_390204), chicken anti-GFP (Aves Labs #GFP-1010, RRID:AB_2307313), and rat anti-CD105/Endoglin (BioLegend #120402, RRID:AB_961070). In addition, Alexa dye-conjugated secondary antibodies were obtained from Thermo Fisher Scientific.

2.3. Tissue processing

To determine the expression levels of the genes in adipose tissues, the tissues were acutely dissected from the mice. The total RNAs were extracted using the RNeasy Mini Lipid Tissue Kit (Qiagen) and were processed for SYBR Green (Thermo Fisher Scientific) qPCR analysis. To examine the appearance of the cold-induced multilocular adipocytes, inguinal WAT were acutely dissected from the mice, fixed in PBS/1% PFA at 4 °C overnight, and processed for paraffin-sectioning and H&E (hematoxylin and eosin) staining.

2.4. 3D volume fluorescence-imaging

Volume fluorescence-imaging was methodologically optimized based on the iDISCO technique and our recently reported procedure [20,22,23]; thus, it is fully compatible with vascular research. The mice of the indicated conditions were anesthetized and perfused with 40 ml PBS/10 μg/ml heparin, and the adipose tissues (i.e., WAT and BAT) were dissected. The tissues were fixed in PBS/1% PFA/10% sucrose at room temperature for 2 h, followed by PBS/1% PFA at room temperature for 2 h. The tissues were washed with PBS for 10 min three times, and the attached connective tissues were completely removed under a dissecting microscope. The tissues were permeabilized with PBS/0.2% TritonX-100/10% DMSO/0.2% Deoxycholate/20 mM EDTA (pH 8.0) at 37 °C for 24 h, and were further permeabilized with PBS/0.2% TritonX-100/10% DMSO/100 mM glycine at 37 °C for 24 h. The tissues were blocked with PBS/0.2% TritonX-100/10% DMSO/5% normal donkey serum at 37 °C for 24 h. The tissues were immunolabeled with the indicated primary antibodies diluted in PBS/0.2% Tween-20/10 μg/ml heparin/5% DMSO/5% normal donkey serum at 37 °C for 48 h, and were washed with PBS/0.2% Tween-20/10 μg/ml heparin at room temperature for 2 h five times. The tissues were subsequently immunolabeled with the corresponding Alexa dye-conjugated secondary antibodies diluted in PBS/0.2% Tween-20/10 μg/ml heparin/5%

DMSO/5% normal donkey serum at 37 °C for 48 h, and were washed with PBS/0.2% Tween-20/10 μg/ml heparin at room temperature for 2 h five times followed by at 37 °C overnight.

For the tissue optical clearing, immunolabeled adipose tissues were embedded in 1% agarose-blocks prepared in PBS. The tissue blocks were dehydrated at room temperature in 20% methanol (diluted in ddH_2O) for 2 h, 40% methanol for 2 h, 60% methanol for 2 h, 80% methanol for 2 h, and 100% methanol for 1 h twice. The tissue blocks were incubated with a mixture of dichloromethane/methanol (2 volumes/1 volume) for 2 h, followed by 100% dichloromethane for 30 min twice. The tissue blocks were ultimately cleared with 100% dibenzyl-ether for 12 h twice to prepare for the 3D volume fluorescence-imaging. The optically cleared adipose tissues were imaged on a LaVisionBiotec Ultramicroscope II equipped with six fixed lightsheet-generating lenses, a CMOS camera (Andor Neo), and a 2 × /NA0.5 objective (MVPLAPO) covered with a 6-mm working-distance dipping-cap. Version v144 of the Inspector Microscope Controller software supported by LaVisionBiotec was used. The tissue blocks were immersed in the chamber filled with 100% dibenzyl-ether for the imaging procedure. For imaging at 1.26× effective magnification (0.63× zoom), the tissue blocks were scanned by the three combined lightsheets, with the step-size of 3 μm through each tissue block. For imaging at 12.6× effective magnification (6.3× zoom), the tissue blocks were scanned by the single lightsheet (middle position), with the step-size of 1 μm through each tissue block. The image stacks were acquired via the continuous lightsheet scanning method without the contrast-blending algorithm.

Imaris (http://www.bitplane.com/imaris/imaris) was used to reconstruct the image stacks obtained from the lightsheet scanning. For display purposes in the figures and movies, a gamma correction of 1.2—1.5 was applied to the raw data. Movies of the image stacks were generated with the frame rate of 30 fps. Perspective or orthogonal 3D projections of the image stacks were generated as indicated for the representative images shown in the figures.

2.5. Statistical methods

To quantify the density of Isolectin-labeled or $CD31^+$ vasculatures in WAT, five 300 μm × 300 μm × 300 μm cubic volumes were randomly selected from the reconstructed 3D images of each tissue, and the length of Isolectin-labeled or CD31-immunolabeled vasculatures in each cubic volume was manually traced. To quantify the density of Isolectin-labeled vasculatures in BAT, four 200 μm × 200 μm × 200 μm cubic volumes were randomly selected from each tissue, and the length of Isolectin-labeled vasculatures in each cubic volume was traced. To quantify the length of vasculatures per adipocyte in WAT, 500 adipocytes immunolabeled by perilipin were randomly selected from each tissue, and the length of surrounding vasculatures was traced. To quantify the density of sympathetic fibers in WAT, six 300 μm × 300 μm × 300 μm cubic volumes were randomly selected from each tissue, and the length of tyrosine hydroxylase-immunolabeled sympathetic fibers in each cubic volume was traced.

Student's two-sided *t*-tests or ANOVAs were performed using GraphPad Prism (http://www.graphpad.com/scientific-software/prism). The statistical details of the experiments are presented in the figure legends.

3. RESULTS

3.1. Three-dimensional volume fluorescence-imaging of the vasculatures in adipose tissues

We sought to utilize 3D volume fluorescence-imaging to examine the vascular network in adipose tissues based on the iDISCO technique and our recently reported procedure [20,22,23]. However, the original methanol-based permeabilization steps used for the whole-mount immunostaining strongly affected several common epitopes for the vasculatures, e.g., CD31/PECAM-1 and CD105/Endoglin (Figs. S1A and S1B). Moreover, the addition of the dichloromethane-mediated delipidation to the methanol-based permeabilization steps, as reported in a similar volume fluorescence-imaging protocol Adipo-Clear [24], completely abolished the immunolabeling of these epitopes (data not shown). Therefore, we methodologically optimized the conditions of whole-mount immunostaining and replaced the methanol-based permeabilization with the detergent-based steps, which effectively preserve the vascular-specific epitopes, such as CD31/PECAM-1 and CD105/Endoglin (Figs. S1A and S1B).

To prove the strengths of this advanced 3D volume fluorescence-imaging technique, we initially labeled the vasculatures in adipose tissues with the colorimetric dye Evans blue via intravenous injection. The intra-adipose vasculatures were largely invisible in the acutely dissected inguinal WAT, whereas they became clearly visualized in the processed tissues (Figure 1A). To examine the delicate network of vasculatures in detail, we exploited the 3D volume fluorescence-imaging on the lightsheet microscope. Alexa dye-conjugated Isolectin GS-IB4, a glycoprotein commonly used in the field to specifically label endothelial cells, was intravenously injected in the mice. Inguinal WAT processed through the imaging procedure indicated a striking pattern of an intra-adipose vascular network on the whole-tissue level at a single-capillary resolution (Figure 1B and Movie S1). Labeling with the intravenously injected 2,000,000 MW-Dextran tetramethylrhodamine, a fluorescent dye that could be largely confined in capillaries because of its high molecular-weight, resulted in the similar pattern of vasculatures in inguinal WAT (Fig. S1C). Importantly, this 3D volume fluorescence-imaging technique with the single-capillary resolution enabled us to accurately quantify the vascular density for the first time in the field (Figure 1E), which was impracticable with conventional immunohistochemistry methods. We showed that the total length of Isolectin-labeled vasculatures in inguinal WAT is 834 ± 57 μm per mm^3 (5 tissues examined), i.e., approximately 0.9 m per mm^3, thus substantiating the claim that adipose tissues are highly vascularized [1—4].

Supplementary data related to this article can be found at https://doi.org/10.1016/j.molmet.2018.06.004.

We subsequently examined the intra-adipose vasculatures through the immunolabeling of intended epitopes. The 3D volume fluorescence-imaging of CD31-immunolabeled inguinal WAT provided the whole-tissue view of the vascular network, as well as the high-magnification view of the vasculatures (Figure 1C,E and Movie S2), similar to those obtained with the intravenously injected fluorescent dyes. In addition, we bred *Tek-Cre* mice, the mouse line to genetically label endothelial cells [25], with *Rosa26-LSL-tdTomato* reporter mice. The whole-tissue network of $tdTomato^+$ vasculatures could be clearly visualized by the 3D volume fluorescence-imaging (Figure 1D). Moreover, this advanced imaging technique is compatible with the purpose of multichannel labeling. The 3D volume fluorescence-imaging of inguinal WAT co-labeled by the intravenously injected fluorescent Isolectin and CD31-immunostaining showed that these two vascular markers largely overlapped as expected (Fig. S1F), i.e., >99.9% $CD31^+$ vasculatures were Isolectin-labeled, whereas 96.3% Isolectin-labeled vasculatures were $CD31^+$ (5 tissues examined). This result is consistent with the notion that Isolectin is normally confined in capillaries because of its specific affinity to endothelial cells and has no interaction with nonvascular structures. Moreover, it is important to note that the procedure of Isolectin-labeling requires approximately

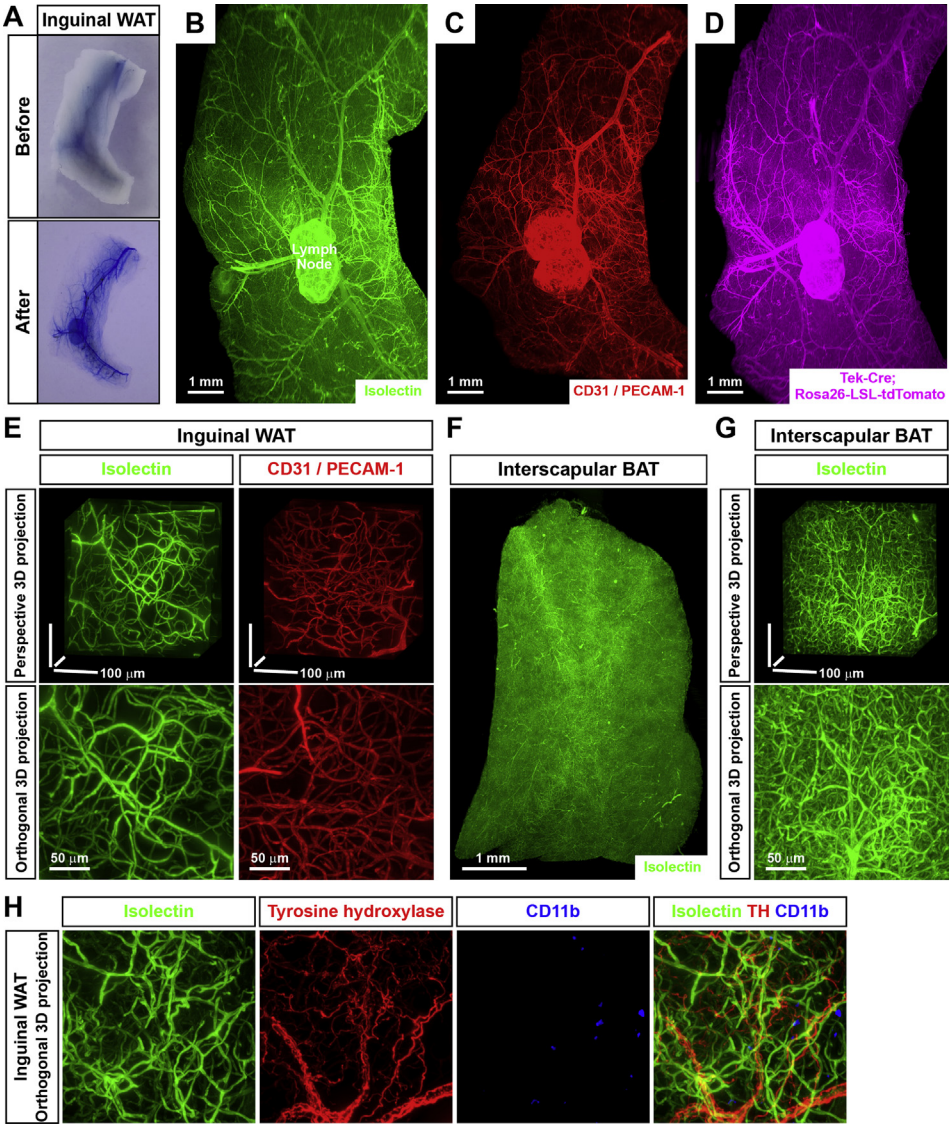

Figure 1: Three-dimensional volume fluorescence-imaging of the vasculatures in mouse adipose tissues. **(A)** The tissue optical clearing for visualization of the vasculatures in adipose tissues. The wild-type mice were intravenously injected with Evans blue. Inguinal WAT before (upper panel) and after (lower panel) the tissue optical clearing. **(B to E)** 3D volume fluorescence-imaging of the vasculatures in WAT. **(B)** The wild-type mice were intravenously injected with Isolectin GS-IB4 Alexa647. Inguinal WAT were processed for the tissue optical clearing and were imaged at 1.26× magnification on the lightsheet microscope. Representative orthogonal 3D-projection image is shown. **(C)** Inguinal WAT of the wild-type mice were processed for the whole-mount immunolabeling of CD31/PECAM-1 and were imaged at 1.26× magnification on the lightsheet microscope. Representative orthogonal 3D-projection image is shown. **(D)** Inguinal WAT of *Tek-Cre*; *Rosa26-LSL-tdTomato* mice were processed for the whole-mount immunolabeling of tdTomato and were imaged at 1.26× magnification on the lightsheet microscope. Representative orthogonal 3D-projection image is shown. **(E)** Isolectin-labeled vasculatures or $CD31^+$ vasculatures in inguinal WAT were imaged at 12.6× magnification on the lightsheet microscope. Representative perspective 3D-projection images of 300 μm × 300 μm × 300 μm cubic tissue volumes (upper panels) or representative orthogonal 3D-projection images of 500 μm-depth tissues (lower panels) are shown. **(F and G)** 3D volume fluorescence-imaging of the vasculatures in BAT. The wild-type mice were intravenously injected with Isolectin GS-IB4 Alexa647. Interscapular BAT were processed for the tissue optical clearing and were imaged at 1.26× **(F)** or 12.6× **(G)** magnification on the lightsheet microscope. **(F)** Representative orthogonal 3D-projection image is shown. **(G)** Representative perspective 3D-projection image of 300 μm × 300 μm × 300 μm cubic tissue volume (upper panel) or representative orthogonal 3D-projection image of 500 μm-depth tissue (lower panel) are shown. **(H)** Simultaneous volume fluorescence-imaging of the vasculatures, the sympathetic arborizations and the immune cells in WAT. The wild-type mice were intravenously injected with Isolectin GS-IB4 Alexa647 (green). Inguinal WAT were processed for the whole-mount co-immunolabeling of tyrosine hydroxylase (red) and CD11b (blue) and were imaged at 12.6× magnification on the lightsheet microscope. Representative orthogonal 3D-projection images of 500 μm-depth tissue are shown.

24 h from the tissue harvesting to the 3D volume fluorescence-imaging. Compared to the procedure of CD31-immunolabeling that requires approximately 8—10 days, the Isolectin-labeling has a clear advantage for research.

Supplementary data related to this article can be found at https://doi.org/10.1016/j.molmet.2018.06.004.

Curiously, the 3D volume fluorescence-imaging of inguinal WAT of *Tek-Cre*; *Rosa26-LSL-tdTomato* mice co-labeled with the intravenously injected fluorescent Isolectin indicated that a portion of Isolectin-labeled vasculatures are tdTomato-negative (Fig. S1G), i.e., >99.9% $tdTomato^+$ vasculatures were Isolectin-labeled, whereas only 89.4% Isolectin-labeled vasculatures were $tdTomato^+$ (5 tissues

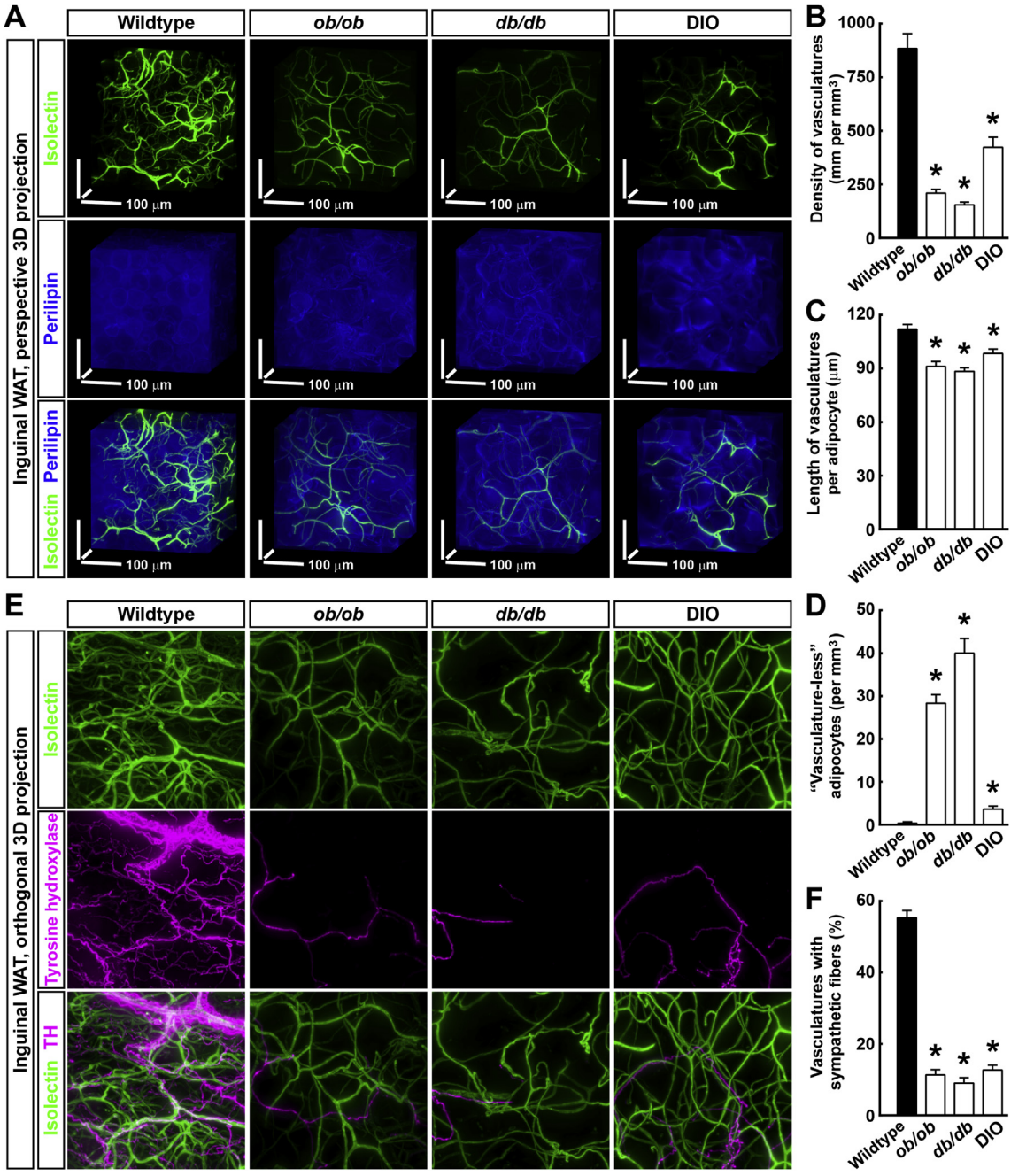

Figure 2: Pathological remodeling of the vasculatures in adipose tissues under obese conditions. **(A to D)** Vascular rarefaction in WAT under the obese conditions. The wild-type, *ob/ob*, *db/db*, and diet-induced obesity (DIO) mice were intravenously injected with Isolectin GS-IB4 Alexa647 (green). Inguinal WAT were processed for the whole-mount immunolabeling of perilipin (blue) and were imaged at 12.6× magnification on the lightsheet microscope. **(A)** Representative perspective 3D-projection images of 300 μm × 300 μm × 300 μm cubic tissue volumes are shown. Density of the vasculatures **(B)**, length of the vasculatures per adipocyte **(C)**, and number of the adipocytes without surrounding vasculatures (i.e., "vasculature-less" adipocytes **D**) were quantified. n = 3, mean ± SEM, $*p < 0.01$. **(E and F)** Disrupted spatial engagement of the sympathetic fibers with the vasculatures under the obese conditions. The wild-type, *ob/ob*, *db/db*, and diet-induced obesity (DIO) mice were intravenously injected with Isolectin GS-IB4 Alexa647 (green). Inguinal WAT were processed for the whole-mount immunolabeling of tyrosine hydroxylase (magenta) and were imaged at 12.6× magnification on the lightsheet microscope. **(E)** Representative orthogonal 3D-projection images of 500 μm-depth tissues are shown. **(F)** Percentage of the vasculatures with sympathetic fibers was quantified. n = 3, mean ± SEM, $*p < 0.01$.

examined). Notably, the intravenously injected fluorescent Isolectin represents the functional assessment of active circulation in the vasculatures. *Tek-Cre*, therefore, appears to incompletely label the vasculatures at least in inguinal WAT, which is likely a result of insufficient Cre-activity in a portion of the endothelial cells. This observation suggests that caution must be taken when utilizing this commonly used genetic tool. In addition, the 3D volume fluorescence-imaging could facilitate examination of the spatial engagement of vasculatures with other components in adipose tissues (refer to subsequent section), e.g., inguinal WAT co-labeled by the intravenously injected

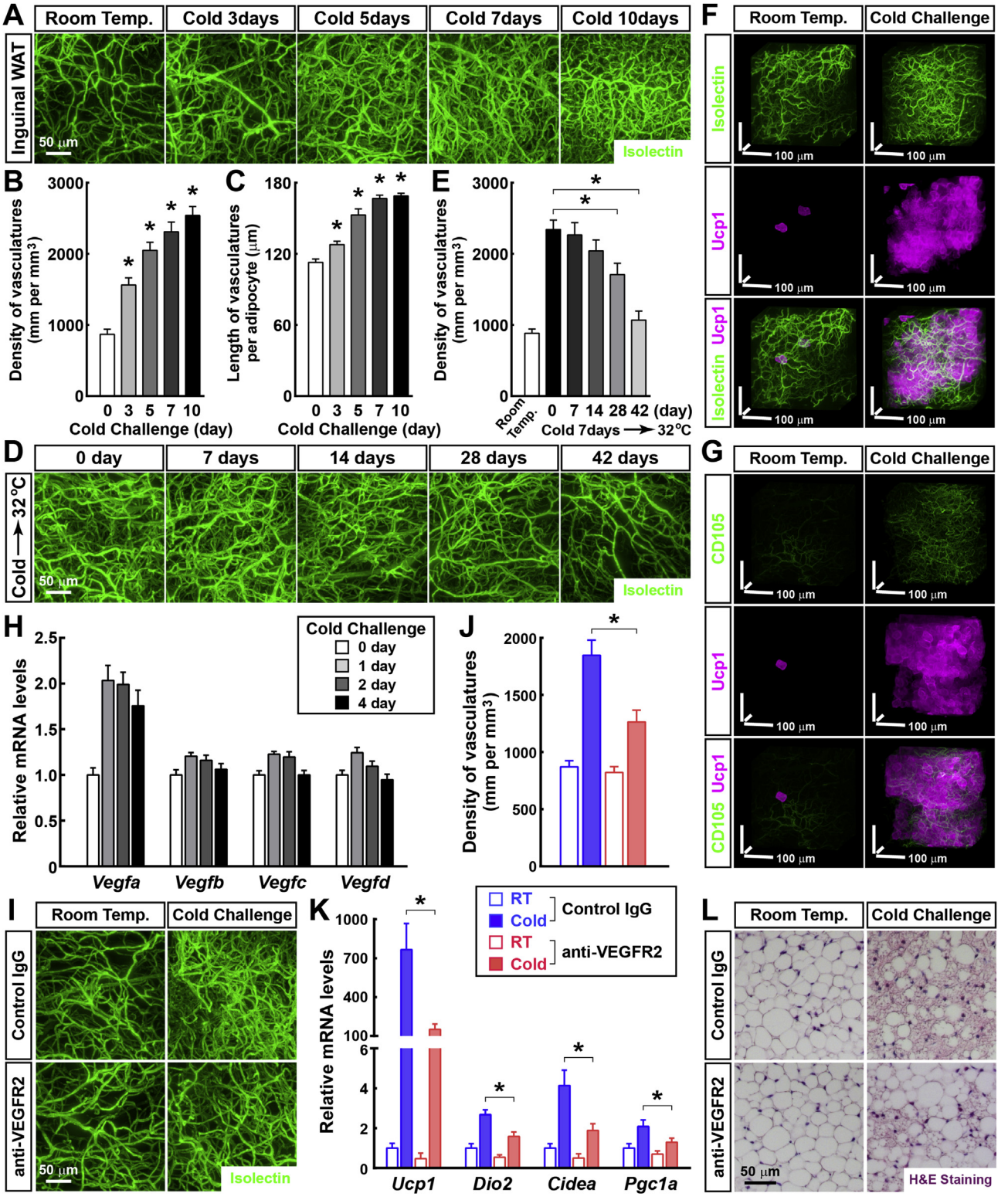

Figure 3: Vascular plasticity in WAT in response to cold challenge. **(A to C)** The vascular plasticity in WAT in response to cold challenge. The wild-type mice were subject to the cold challenge (4 °C) and were intravenously injected with Isolectin GS-IB4 Alexa647 at the indicated time points. Inguinal WAT were processed for the tissue optical clearing and were imaged at 12.6× magnification on the lightsheet microscope. **(A)** Representative orthogonal 3D-projection images of 500 μm-depth tissues are shown. Density of the vasculatures **(B)** and length of the vasculatures per adipocyte **(C)** were quantified. n = 4, mean ± SEM, *$p < 0.01$. **(D and E)** The cold-induced vascular plasticity is reversible. The wild-type mice were subject to cold challenge for 7 days and then reacclimated at the thermal-neutral condition (32 °C). The mice were intravenously injected with Isolectin GS-IB4 Alexa647 at the indicated time points. Inguinal WAT were processed for the tissue optical clearing and were imaged at 12.6× magnification on the lightsheet microscope. **(D)** Representative orthogonal 3D-projection images of 500 μm-depth tissues are shown. **(E)** Density of the vasculatures was quantified. n = 4, mean ± SEM, *$p < 0.01$. **(F and G)** The cold-induced vascular plasticity is functionally connected with the beiging process of WAT. *Ucp1*$^{CreERT2/+}$; *Rosa26-LSL-EGFP* mice daily treated with 4-hydroxytamoxifen

fluorescent Isolectin, tyrosine hydroxylase-immunostaining for sympathetic fibers, and CD11b-immunostaining for immune cells (Figure 1H).

This 3D volume fluorescence-imaging technique is readily applicable to different adipose depots. For example, the entirety of the vascular network and the delicate distribution of vasculatures in perigonadal WAT were visualized via the intravenously injected fluorescent Isolectin (Figs. S1D and S1E). Detailed quantification showed that the density of the vasculatures in perigonadal WAT is 625 $\pm$ 48 μm per mm^3 (5 tissues examined), approximately 25% lower than that in inguinal WAT. Furthermore, the vascular network in interscapular BAT was determined by the 3D volume fluorescence-imaging (Figure 1F,G and Movie S3). The vasculatures in the interscapular BAT reach a strikingly high density of 14,350 $\pm$ 550 μm per mm^3 (5 tissues examined), equivalent to greater than 14 m per mm^3 and approximately 15-fold higher than that in inguinal WAT.

Supplementary data related to this article can be found at https://doi.org/10.1016/j.molmet.2018.06.004.

Taken together, these results have demonstrated the 3D volume fluorescence-imaging technique that enables the whole-tissue visualization and accurate quantification of the vasculatures in adipose tissues for the first time in the field.

3.2. Pathological remodeling of the vasculatures in adipose tissues under obese conditions

To further exhibit the strength of 3D volume fluorescence-imaging of the vasculatures, we aimed to characterize their pathological remodeling process in obese conditions. We examined the inguinal WAT of the wild-type, *ob/ob*, *db/db*, and diet-induced obesity (DIO) mice, co-labeled by the intravenously injected fluorescent Isolectin and the whole-mount immunostaining of perilipin, a specific cellular marker for adipocytes (Figure 2A). In line with the previous findings [26], there was a substantial decrease of the vascular density, i.e., vascular rarefaction, in the *ob/ob*, *db/db*, and DIO mice. Detailed quantification showed that the density of the vasculatures was 884 $\pm$ 69 μm per mm^3 in the wild-type, 210 $\pm$ 18 μm per mm^3 in the *ob/ob*, 155 $\pm$ 13 μm per mm^3 in the *db/db*, and 423 $\pm$ 47 μm per mm^3 in the DIO mice (Figure 2B). We did not identify a significant change in the average diameter of the capillaries in the *ob/ob*, *db/db*, and DIO mice compared to that in the wild-type mice (Figure 2A). The 3D volume fluorescence-imaging of CD31-immunolabeled inguinal WAT of the wild-type, *ob/ob*, *db/db*, and DIO mice yielded similar results (Fig. S2B). Because the size of the adipocytes significantly increased in the obese conditions (Figure 2A), the average length of the vasculatures per adipocyte was also quantified. Compared to the wild-type mice, the *ob/ob*, *db/db* and DIO mice all showed decreased lengths of the vasculatures per adipocyte in the inguinal WAT (Figure 2C), although to less extent than that observed with the overall vascular density. In addition, the process of vascular rarefaction occurred in the interscapular BAT under the obese conditions (Fig. S2D), in agreement with previous findings [27]. Quantification showed that the density of the Isolectin-labeled vasculatures in the interscapular BAT was 14,290 $\pm$ 450 μm per mm^3 in the wild-type, 1157 $\pm$ 86 μm per mm^3 in the *db/db*, and 2195 $\pm$ 219 μm per mm^3 in the DIO mice (Fig. S2E). Interestingly, >99.9% adipocytes (10,000 adipocytes examined) in the inguinal WAT of the wild-type mice appeared in close apposition to capillaries, in accordance with the existing literature [1–4]. However, a small portion of adipocytes in the obese conditions completely lost their direct contact with capillaries (Figure 2D and Fig. S2A). The 3D volume fluorescence-imaging enabled us to observe these "vasculature-less" adipocytes that had been undetected by conventional methods. Although these "vasculature-less" adipocytes exhibited a similar cell size compared to that of the surrounding adipocytes (Fig. S2A), they might undergo hypoxia and exhibit altered metabolism. Future studies are warranted to elucidate in detail the cell biology of these new "vasculature-less" adipocytes.

We recently showed that the sympathetic arborizations in WAT diminished in the obese conditions [23]. To examine whether the vascular rarefaction would correlate with this obesity-related sympathetic atrophy, we examined the inguinal WAT of the wild-type, *ob/ob*, *db/db*, and DIO mice, co-labeled by the intravenously injected fluorescent Isolectin and the whole-mount immunostaining of tyrosine hydroxylase, a specific marker for the sympathetic fibers (Figure 2E). Consistent with our previous finding, the sympathetic arborizations substantially decreased in the *ob/ob*, *db/db*, and DIO mice as indicated by the 3D volume fluorescence-imaging. Quantification showed that the density of the sympathetic fibers in the inguinal WAT was 535 $\pm$ 37 μm per mm^3 in the wild-type (i.e., approximately 0.5 m per mm^3), 65 $\pm$ 9 μm per mm^3 in the *ob/ob*, 50 $\pm$ 8 μm per mm^3 in the *db/db*, and 100 $\pm$ 12 μm per mm^3 in the DIO mice (Fig. S2C). Furthermore, detailed examination showed that there was a significant spatial engagement between the sympathetic arborizations and the vasculatures in the inguinal WAT of the wild-type mice (Figure 2E and Movie S4), with more than 50% of the vasculatures having sympathetic fibers traveling alongside (Figure 2F). Intriguingly, this spatial engagement of the vasculatures with the sympathetic arborizations was disrupted in the *ob/ob*, *db/db*, and DIO mice (Figure 2E,F). The 3D volume fluorescence-imaging has therefore revealed another new feature in the pathological remodeling of intra-adipose vasculatures under obese conditions.

Supplementary data related to this article can be found at https://doi.org/10.1016/j.molmet.2018.06.004.

Furthermore, the 3D volume fluorescence-imaging technique could be utilized to assess the leakage of capillaries in adipose tissues, which occurs under the obese conditions [28]. The mice were intravenously injected with 2,000,000 MW-Dextran tetramethylrhodamine, which should be normally confined in capillaries because of its high molecular-weight. The mice were then thoroughly perfused with

were maintained at room temperature or subjected to cold challenge. **(F)** The mice were intravenously injected with Isolectin GS-IB4 Alexa647 (green). Inguinal WAT were processed for the whole-mount immunolabeling of EGFP (magenta) and were imaged at 12.6× magnification on the lightsheet microscope. Representative perspective 3D-projection images of 300 μm × 300 μm × 300 μm cubic tissue volumes are shown. **(G)** Inguinal WAT were processed for the whole-mount co-immunolabeling of CD105/Endoglin (green) and EGFP (magenta) and were imaged at 12.6× magnification on the lightsheet microscope. Representative perspective 3D-projection images of 300 μm × 300 μm × 300 μm cubic tissue volumes are shown. **(H)** The cold-induced expression of *Vegf* genes in WAT. The wild-type mice were subjected to cold challenge, and inguinal WAT were harvested at the indicated time points. Expression levels of *Vegf* genes were examined via qPCR analysis. n = 4, mean $\pm$ SEM. **(I to L)** The cold-induced vascular plasticity is involved in the beiging process of WAT. The wild-type mice administered VEGFR2-neutralizing antibody or control IgG were maintained at room temperature or subjected to cold challenge. **(I and J)** The mice were then intravenously injected with Isolectin GS-IB4 Alexa647. Inguinal WAT were processed for tissue optical clearing and were imaged at 12.6× magnification on the lightsheet microscope. **(I)** Representative orthogonal 3D-projection images of 500 μm-depth tissues are shown. **(J)** Density of the vasculatures was quantified. n = 5, mean $\pm$ SEM, $*p < 0.01$. **(K)** Expression levels of the beiging-related genes in the inguinal WAT were examined via qPCR analysis. n = 5, mean $\pm$ SEM, $*p < 0.01$. **(L)** Appearance of multilocular adipocytes in the inguinal WAT was examined via H&E staining.

phosphate-buffered saline to wash out the fluorescent dye from the vascular system. As expected, the 3D volume fluorescence-imaging of the inguinal WAT of the wild-type mice showed little fluorescence signal remaining (Fig. S2F). In contrast, the inguinal WAT of the *db/db* and DIO mice exhibited significant leakage of the fluorescent dye from the capillaries, as evidenced by the fluorescence-labeled cells in the tissues (Fig. S2F).

Together, these results have provided the fine characterization of the pathological remodeling of vasculatures in adipose tissues, thus demonstrating the research power of this 3D volume fluorescence-imaging procedure.

3.3. Sympathetic-derived catecholamine signal regulates the cold-induced vascular plasticity in WAT

We subsequently aimed to assess the physiological vascular plasticity in WAT in response to a cold challenge (4 °C) using 3D volume fluorescence-imaging. We examined the vasculatures in the inguinal WAT of the cold-challenged wild-type mice, labeled by the intravenously injected fluorescent Isolectin. In line with previous studies [29,30], there was a significant increase in the vascular density as early as 3 days after the cold challenge (Figure 3A). Detailed quantification showed that the density of the vasculatures in the inguinal WAT was 867 ± 73 μm per mm^3 at 0 day, 1551 ± 99 μm per mm^3 at 3 days, 2048 ± 112 μm per mm^3 at 5 days, 2309 ± 138 μm per mm^3 at 7 days, and 2539 ± 126 μm per mm^3 at 10 days after the cold challenge (Figure 3B). We did not identify a significant change in the average diameter of the capillaries in response to the cold challenge (Figure 3A). The 3D volume fluorescence-imaging of the CD31-immunolabeled inguinal WAT of the cold-challenged wild-type mice provided similar results (Fig. S3A). Because the size of the adipocytes decreased in the inguinal WAT after the cold challenge, the average length of the vasculatures per adipocyte was also quantified. The length of the vasculatures per adipocyte in the inguinal WAT significantly increased in response to the cold challenge (Figure 3C). We subsequently examined whether this cold-induced vascular plasticity would be reversible. The wild-type mice were reacclimated at the thermal-neutral condition (32 °C) following cold challenge for 7 days. We examined their inguinal WAT labeled by the intravenously injected fluorescent Isolectin. Interestingly, 2 weeks after the thermal-neutral condition, the vascular density began to decrease (Figure 3D). Quantification showed that 6 weeks after the thermal-neutral condition, the density of the vasculatures in the inguinal WAT returned to the baseline level of the mice maintained at room temperature (Figure 3E). The 3D volume fluorescence-imaging of the CD31-immunolabeled inguinal WAT showed similar results (Fig. S3B), which demonstrates that the cold-induced vascular plasticity in WAT is completely reversible.

Recent studies in the field have shown that WAT can undergo the beiging (or browning) process, i.e., the appearance of Ucp1-positive multilocular adipocytes, in response to a cold challenge. The beiging process results in the enhanced energy expenditure and has increasingly gained attention for its potential therapeutic application in obesity and type 2 diabetes [8,31–33]. We therefore explored the functional connection between the cold-induced vascular plasticity and the beiging process of WAT. We generated the *Ucp1*$^{CreERT2/+}$ knock-in mouse line (Fig. S3C) and bred it with *Rosa26-LSL-EGFP* reporter mice. The *Ucp1*$^{CreERT2/+}$; *Rosa26-LSL-EGFP* mice were maintained at room temperature or were subject to the cold challenge, and the Cre-recombinase activity was induced with 4-hydroxytamoxifen. We performed the 3D volume fluorescence-imaging of the inguinal WAT co-labeled by the intravenously injected fluorescent Isolectin and the whole-mount immunostaining of EGFP. The *Ucp1*$^{CreERT2/+}$; *Rosa26-LSL-EGFP* mice maintained at room temperature showed a limited number of Ucp1/EGFP-positive cells in their inguinal WAT, consistent with the scarcity of brown or beige adipocytes under the ambient condition (Figure 3F). In contrast, the cold-challenged *Ucp1*$^{CreERT2/+}$; *Rosa26-LSL-EGFP* mice exhibited a massive accumulation of Ucp1/EGFP-positive cells in the inguinal WAT (Figure 3F). Importantly, the detailed view showed that these Ucp1/EGFP-positive cells in the cold-challenged inguinal WAT were in close apposition to the increased vasculatures (Figure 3F and Movie S5). Moreover, we analyzed the inguinal WAT of the *Ucp1*$^{CreERT2/+}$; *Rosa26-LSL-EGFP* mice via whole-mount co-immunostaining of EGFP and CD105/Endoglin, a cellular marker for angiogenesis [34]. The intensity of the CD105-immunolabeling was relatively low under the room temperature condition, whereas it significantly increased after the cold challenge (Figure 3G and Fig. S3D). In addition, $CD105^+$ vasculatures appeared spatially associated with the Ucp1/EGFP-positive cells in the cold-challenged inguinal WAT (Figure 3G), which suggests that angiogenesis is likely involved in the beiging process.

Supplementary data related to this article can be found at https://doi.org/10.1016/j.molmet.2018.06.004.

Consistent with the increased vascular density and angiogenesis in the cold-challenged inguinal WAT, upregulation of the expression of *Vegf* genes, particularly *Vegfa*, was identified (Figure 3H). A previous study demonstrated that the VEGFR2 signal is essential for the cold-induced angiogenesis in WAT [30]. Therefore, we administered VEGFR2-neutralizing antibody to the wild-type mice (i.e., VEGFR2-blocked mice), and the mice were subsequently maintained at room temperature or subjected to the cold challenge. Compared with the mice administered the control IgG, the VEGFR2-blocked mice maintained at room temperature exhibited a similar vascular density in their inguinal or perigonadal WAT for at least 5 days, as indicated by the 3D volume fluorescence-imaging (Figure 3I, 3J, Fig. S3E and S3F). However, the cold-induced vascular plasticity was significantly inhibited in the inguinal or perigonadal WAT of the VEGFR2-blocked mice (Figure 3I, 3J, Fig. S3E and S3F). More importantly, this inhibition of the vascular plasticity resulted in the suppression of the beiging process in the inguinal WAT, as assessed by the qPCR analysis of beiging-related genes (Figure 3K) and the histochemical examination of multilocular adipocytes (Figure 3L), which suggests that the vascular plasticity is involved in the cold-induced beiging process of WAT.

We subsequently explored the physiological mechanism that underlies the cold-induced vascular plasticity in WAT. Previous studies have reported that catecholamines might promote *Vegfa* expression in adipose tissues [35,36]. Because we observed the spatial engagement between the sympathetic arborizations and the vasculatures in WAT (Figure 2E), we examined whether the sympathetic-derived catecholamine signal would regulate the cold-induced vascular plasticity. We recently showed that the sympathetic arborizations in WAT depend on the TrkA signal, and *Th-Cre*;*TrkA*$^{fl/fl}$ mice lose the majority of intra-adipose sympathetic arborizations in their inguinal WAT (Fig. S4A) [23]. Interestingly, we determined that compared to the control *Th-Cre*;*TrkA*$^{+/+}$ mice, the cold-induced upregulation of *Vegfa* expression was inhibited in the inguinal WAT of the *Th-Cre*;*TrkA*$^{fl/fl}$ mice (Figure 4B). Accordingly, the cold-induced vascular plasticity was suppressed in the inguinal WAT of the *Th-Cre*;*TrkA*$^{fl/fl}$ mice, as indicated by the 3D volume fluorescence-imaging of Isolectin-labeled or CD31-immunolabeled vasculatures (Figure 4A,C and Fig. S4B). In parallel with this approach of genetic ablation, we also locally treated the inguinal WAT of the wild-type mice with 6-hydroxydopamine (6-OHDA) to pharmacologically destroy their sympathetic arborizations (Fig. S4C). Similar to the findings obtained with *Th-Cre*;*TrkA*$^{fl/fl}$

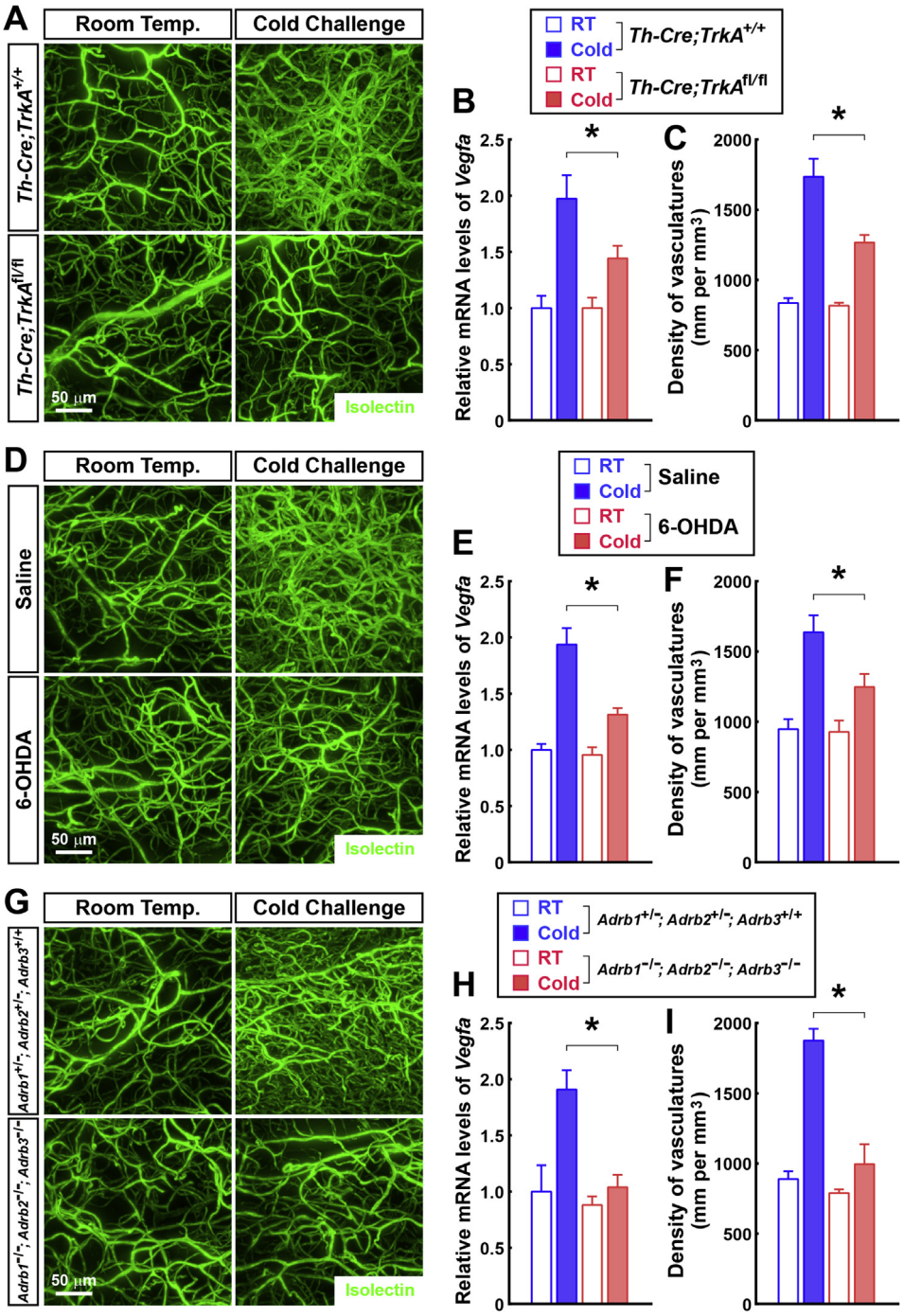

Figure 4: Cold-induced vascular plasticity in WAT depends on the sympathetic-derived catecholamine signal. **(A to C)** Genetic ablation of the intra-adipose sympathetic arborizations inhibits the cold-induced vascular plasticity in WAT. *Th-Cre;TrkA*$^{+/+}$ or *Th-Cre;TrkA*$^{fl/fl}$ mice were maintained at room temperature or subjected to cold challenge. **(A and C)** The mice were then intravenously injected with Isolectin GS-IB4 Alexa647. Inguinal WAT were processed for the tissue optical clearing and were imaged at 12.6× magnification on the lightsheet microscope. **(A)** Representative orthogonal 3D-projection images of 500 μm-depth tissues are shown. **(C)** Density of the vasculatures was quantified. n = 4, mean ± SEM, *$p < 0.01$. **(B)** Expression levels of *Vegfa* gene were examined via qPCR analysis. n = 4, mean ± SEM, *$p < 0.01$. **(D to F)** Local pharmacologic ablation of the sympathetic arborizations suppresses the cold-induced vascular plasticity in WAT. Inguinal WAT of the wild-type mice were locally treated with 6-hydroxydopamine (6-OHDA) or saline control, and the mice were subjected to cold challenge at 6 days after the treatment. **(D and F)** The mice were then intravenously injected with Isolectin GS-IB4 Alexa647. Inguinal WAT were processed for tissue optical clearing and were imaged at 12.6× magnification on the lightsheet microscope. **(D)** Representative orthogonal 3D-projection images of 500 μm-depth tissues are shown. **(F)** Density of the vasculatures was quantified. n = 5, mean ± SEM, *$p < 0.01$. **(E)** Expression levels of *Vegfa* gene were examined via qPCR analysis. n = 5, mean ± SEM, *$p < 0.01$. **(G to I)** The cold-induced vascular plasticity depends on the catecholamine signal. *Adrb1*$^{+/-}$; *Adrb2*$^{+/-}$; *Adrb3*$^{+/+}$ or *Adrb1*$^{-/-}$; *Adrb2*$^{-/-}$; *Adrb3*$^{-/-}$ mice were maintained at room temperature or subjected to cold challenge. **(G and I)** The mice were then intravenously injected with Isolectin GS-IB4 Alexa647. Inguinal WAT were processed for tissue optical clearing and were imaged at 12.6× magnification on the lightsheet microscope. **(G)** Representative orthogonal 3D-projection images of 500 μm-depth tissues are shown. **(I)** Density of the vasculatures was quantified. n = 5, mean ± SEM, *$p < 0.01$. **(H)** Expression levels of *Vegfa* gene were examined via qPCR analysis. n = 5, mean ± SEM, *$p < 0.01$.

mice, the cold-induced upregulation of the *Vegfa* expression was inhibited in the 6-OHDA-treated inguinal WAT compared to the saline-treated control (Figure 4E). In addition, the cold-induced vascular plasticity was suppressed in the 6-OHDA-treated inguinal WAT (Figure 4D,F and Fig. S4D). Catecholamines trigger the activation of β-adrenergic receptors (β1, β2, and β3). We further utilized *Adrb1*$^{-/-}$; *Adrb2*$^{-/-}$; *Adrb3*$^{-/-}$ mice, in which all three genes of β-adrenergic receptors are deleted. Compared to the control *Adrb1*$^{+/-}$; *Adrb2*$^{+/-}$; *Adrb3*$^{+/+}$ mice, the cold-induced *Vegfa* upregulation in the inguinal WAT was completely suppressed in the *Adrb1*$^{-/-}$; *Adrb2*$^{-/-}$; *Adrb3*$^{-/-}$ mice (Figure 4H). Moreover, the cold-induced vascular plasticity was largely abolished in the *Adrb1*$^{-/-}$; *Adrb2*$^{-/-}$; *Adrb3*$^{-/-}$ mice (Figure 4G,I and Fig. S4E). Together, these results have demonstrated that the sympathetic-derived catecholamine signal is required for the cold-induced vascular plasticity in WAT.

Overall, the 3D volume fluorescence-imaging technique has shown the significant, and reversible, vascular plasticity in WAT in response to a cold challenge. These physiological changes of vasculatures depend on the sympathetic-derived catecholamine signal and are involved in the cold-induced beiging process.

4. DISCUSSION

In this study, we report on 3D volume fluorescence-imaging procedure to visualize the entirety of the vascular network in mouse adipose tissues. To our knowledge, this work represents the first example in the field in which the vasculatures are revealed, and accurately quantified, on the whole-tissue level with a single-capillary resolution. Importantly, the new imaging procedure has overcome the common limitations of conventional immunohistochemistry, i.e., sample size and 3D field view. This technical advance would be compatible with divergent purposes of the research on vasculatures in adipose tissues, as well as in other organs in general. We have proven its strengths in assessing the pathological remodeling of intra-adipose vasculatures under obese conditions, as well as the physiological increase of vasculatures in the context of a cold challenge. The results have not only substantiated the prior observations from conventional immunohistochemistry methods but have also elucidated several new features in the vascular plasticity. For example, the 3D volume fluorescence-imaging of WAT in the obese conditions indicated for the first time the existence of "vasculature-less" adipocytes. Future studies will help elucidate whether these adipocytes might undergo hypoxia and exhibit altered metabolism. This advanced imaging technique has therefore opened the avenue to more research applications.

Extending our recent finding of the dense sympathetic arborizations in WAT [23], we determined that the sympathetic arborizations appear spatially engaged with more than 50% of the vasculatures in WAT. Furthermore, we have shown that the sympathetic-derived catecholamine signal exerts an essential role in the cold-induced vascular plasticity, with genetic or pharmacologic ablation of the intra-adipose sympathetic arborizations significantly inhibiting the cold-induced *Vegfa* expression and increase of the vascular density. Similarly, genetic deletion of the three β-adrenergic receptors completely suppresses the cold-induced vascular plasticity in WAT. Our results have together suggested a functional interaction between the sympathetic and vascular systems in WAT in response to a cold challenge; but the molecular mechanism that underlies the catecholamine-stimulated *Vegfa* expression remains to be explored in detail, which likely involves the cAMP/protein kinase A signal downstream of β-adrenergic receptors [36]. In addition, previous reports have documented the increase of vascular density in WAT after a cold challenge [29,30]. We further showed that this cold-induced vascular plasticity is coupled with the beiging process of WAT, i.e., the appearance of Ucp1-positive multilocular adipocytes: (1) the increase of the vascular density, as well as the cold-induced angiogenesis, is spatially associated with the Ucp1-positive adipocytes as revealed with the newly generated *Ucp1*$^{CreERT2/+}$ reporter line; (2) blockage of the VEGFR2 signal effectively inhibits the upregulation of beiging-related genes and the appearance of multilocular adipocytes in WAT. These results have demonstrated that the vascular plasticity, regulated by the sympathetic-derived catecholamine signal, is involved in this cold-induced metabolic event of WAT, which suggests the intriguing interplay between vascular, neural and metabolic systems.

Furthermore, we previously showed that the density of the sympathetic arborizations in WAT substantially decreased in obese conditions [23], a striking phenomenon that we have confirmed and accurately quantified in this study. Moreover, the new imaging power has illustrated that this obesity-related sympathetic atrophy in WAT appears to correlate with the disruption of the sympathetic engagement with the vasculatures, as well as the decrease of the vascular density. It becomes tempting to speculate that a causative relationship between these two pathological events might exist, e.g., the loss of the sympathetic efferent inputs results in the vascular rarefaction, which might represent a synergetic mechanism in the destruction of the metabolic homeostasis of WAT in obese conditions. Future research efforts are needed to explore these exciting possibilities.

5. CONCLUSIONS

We report a new 3D volume fluorescence-imaging procedure that is compatible with divergent purposes of the research on vasculatures, which is poised to serve the field in future investigations on the vascular system in adipose tissues or other research scenarios.

ACKNOWLEDGMENTS

This work was supported by the National Natural Science Foundation of China (31770936 and 91742106) to W.Z., the Beijing Natural Science Foundation (5172016) to W.Z., the Thousand-Talent Young Investigator Program to W.Z., and the National Key R&D Program of China (2017YFA0505800). The Zeng laboratory was also supported by the Center for Life Sciences, the Institute for Immunology, and the School of Medicine at Tsinghua University.

Y.C. and H.W. contributed equally to this work. W.Z. is the senior and corresponding author. W.Z. conceived and designed the project. Y.C., H.W., Q.W., and X.H. performed and analyzed the experiments with input from W.Z. The manuscript was written by W.Z. with the assistance of Y.C. and H.W.

DECLARATIONS OF INTEREST

None.

APPENDIX A. SUPPLEMENTARY DATA

Supplementary data related to this article can be found at https://doi.org/10.1016/j.molmet.2018.06.004.

REFERENCES

[1] Cao, Y., Sep 2007. Angiogenesis modulates adipogenesis and obesity. Journal of Clinical Investigation 117:2362–2368.

[2] Neels, J.G., Thinnes, T., Loskutoff, D.J., Jun 2004. Angiogenesis in an in vivo model of adipose tissue development. The FASEB Journal 18:983–985.

[3] Crandall, D.L., Hausman, G.J., Kral, J.G., Jun 1997. A review of the microcirculation of adipose tissue: anatomic, metabolic, and angiogenic perspectives. Microcirculation 4:211–232.
[4] Napolitano, L., Sep 1963. The differentiation of white adipose cells. An electron microscope study. The Journal of Cell Biology 18:663–679.
[5] Reilly, S.M., Saltiel, A.R., Nov 2017. Adapting to obesity with adipose tissue inflammation. Nature Reviews Endocrinology 13:633–643.
[6] Czech, M.P., Jul 11 2017. Insulin action and resistance in obesity and type 2 diabetes. Nature Medicine 23:804–814.
[7] Kusminski, C.M., Bickel, P.E., Scherer, P.E., Sep 2016. Targeting adipose tissue in the treatment of obesity-associated diabetes. Nature Reviews Drug Discovery 15:639–660.
[8] Rosen, E.D., Spiegelman, B.M., Jan 16 2014. What we talk about when we talk about fat. Cell 156:20–44.
[9] Augustin, H.G., Koh, G.Y., Aug 25 2017. Organotypic vasculature: from descriptive heterogeneity to functional pathophysiology. Science 357.
[10] Cao, Y., Oct 1 2013. Angiogenesis and vascular functions in modulation of obesity, adipose metabolism, and insulin sensitivity. Cell Metabolism 18:478–489.
[11] Sun, K., Kusminski, C.M., Scherer, P.E., Jun 2011. Adipose tissue remodeling and obesity. Journal of Clinical Investigation 121:2094–2101.
[12] Cao, Y., Feb 2010. Adipose tissue angiogenesis as a therapeutic target for obesity and metabolic diseases. Nature Reviews Drug Discovery 9:107–115.
[13] Park, J., Kim, M., Sun, K., An, Y.A., Gu, X., Scherer, P.E., Jun 2017. Vegf-a-expressing adipose tissue shows rapid beiging and enhanced survival after transplantation and confers IL-4-independent metabolic improvements. Diabetes 66:1479–1490.
[14] Robciuc, M.R., Kivela, R., Williams, I.M., de Boer, J.F., van Dijk, T.H., Elamaa, H., et al., Apr 12 2016. VEGFB/VEGFR1-Induced expansion of adipose vasculature counteracts obesity and related metabolic complications. Cell Metabolism 23:712–724.
[15] Honek, J., Seki, T., Iwamoto, H., Fischer, C., Li, J., Lim, S., et al., Oct 14 2014. Modulation of age-related insulin sensitivity by VEGF-dependent vascular plasticity in adipose tissues. Proceedings of the National Academy of Sciences U S A 111:14906–14911.
[16] Sung, H.K., Doh, K.O., Son, J.E., Park, J.G., Bae, Y., Choi, S., et al., Jan 8 2013. Adipose vascular endothelial growth factor regulates metabolic homeostasis through angiogenesis. Cell Metabolism 17:61–72.
[17] Sun, K., Wernstedt Asterholm, I., Kusminski, C.M., Bueno, A.C., Wang, Z.V., Pollard, J.W., et al., Apr 10 2012. Dichotomous effects of VEGF-A on adipose tissue dysfunction. Proceedings of the National Academy of Sciences U S A 109:5874–5879.
[18] Elias, I., Franckhauser, S., Ferre, T., Vila, L., Tafuro, S., Munoz, S., et al., Jul 2012. Adipose tissue overexpression of vascular endothelial growth factor protects against diet-induced obesity and insulin resistance. Diabetes 61:1801–1813.
[19] Rupnick, M.A., Panigrahy, D., Zhang, C.Y., Dallabrida, S.M., Lowell, B.B., Langer, R., et al., Aug 6 2002. Adipose tissue mass can be regulated through the vasculature. Proceedings of the National Academy of Sciences U S A 99:10730–10735.
[20] Renier, N., Wu, Z., Simon, D.J., Yang, J., Ariel, P., Tessier-Lavigne, M., Nov 06 2014. iDISCO: a simple, rapid method to immunolabel large tissue samples for volume imaging. Cell 159:896–910.
[21] Belle, M., Godefroy, D., Dominici, C., Heitz-Marchaland, C., Zelina, P., Hellal, F., et al., Nov 20 2014. A simple method for 3D analysis of immunolabeled axonal tracts in a transparent nervous system. Cell Reports 9:1191–1201.
[22] Cao, Y., Wang, H., Zeng, W., Mar 27 2018. Whole-tissue 3D imaging reveals intra-adipose sympathetic plasticity regulated by NGF-TrkA signal in cold-induced beiging. Protein Cell 9(6):527–539.
[23] Jiang, H., Ding, X., Cao, Y., Wang, H., Zeng, W., Oct 03 2017. Dense intra-adipose sympathetic arborizations are essential for cold-induced beiging of mouse white adipose tissue. Cell Metabolism 26, pp. 686–692 e3.
[24] Chi, J., Wu, Z., Choi, C.H.J., Nguyen, L., Tegegne, S., Ackerman, S.E., et al., Jan 9 2018. Three-dimensional adipose tissue imaging reveals regional variation in beige fat biogenesis and PRDM16-dependent sympathetic neurite density. Cell Metabolism 27, pp. 226–236 e3.
[25] Kisanuki, Y.Y., Hammer, R.E., Miyazaki, J., Williams, S.C., Richardson, J.A., Yanagisawa, M., Feb 15 2001. Tie2-Cre transgenic mice: a new model for endothelial cell-lineage analysis in vivo. Developmental Biology 230:230–242.
[26] Voros, G., Maquoi, E., Demeulemeester, D., Clerx, N., Collen, D., Lijnen, H.R., Oct 2005. Modulation of angiogenesis during adipose tissue development in murine models of obesity. Endocrinology 146:4545–4554.
[27] Shimizu, I., Aprahamian, T., Kikuchi, R., Shimizu, A., Papanicolaou, K.N., MacLauchlan, S., et al., May 2014. Vascular rarefaction mediates whitening of brown fat in obesity. Journal of Clinical Investigation 124:2099–2112.
[28] Scalia, R., Mar 2013. The microcirculation in adipose tissue inflammation. Reviews in Endocrine & Metabolic Disorders 14:69–76.
[29] Luo, X., Jia, R., Luo, X.Q., Wang, G., Zhang, Q.L., Qiao, H., et al., 2017. Cold exposure differentially stimulates angiogenesis in BAT and WAT of mice: implication in adrenergic activation. Cellular Physiology and Biochemistry 42:974–986.
[30] Xue, Y., Petrovic, N., Cao, R., Larsson, O., Lim, S., Chen, S., et al., Jan 7 2009. Hypoxia-independent angiogenesis in adipose tissues during cold acclimation. Cell Metabolism 9:99–109.
[31] Giordano, A., Frontini, A., Cinti, S., Jun 2016. Convertible visceral fat as a therapeutic target to curb obesity. Nature Reviews Drug Discovery 15:405–424.
[32] Kajimura, S., Spiegelman, B.M., Seale, P., Oct 06 2015. Brown and beige fat: physiological roles beyond heat generation. Cell Metabolism 22:546–559.
[33] Peirce, V., Carobbio, S., Vidal-Puig, A., Jun 05 2014. The different shades of fat. Nature 510:76–83.
[34] Dallas, N.A., Samuel, S., Xia, L., Fan, F., Gray, M.J., Lim, S.J., et al., Apr 1 2008. Endoglin (CD105): a marker of tumor vasculature and potential target for therapy. Clinical Cancer Research 14:1931–1937.
[35] Fredriksson, J.M., Nikami, H., Nedergaard, J., Oct 24 2005. Cold-induced expression of the VEGF gene in brown adipose tissue is independent of thermogenic oxygen consumption. FEBS Letters 579:5680–5684.
[36] Fredriksson, J.M., Lindquist, J.M., Bronnikov, G.E., Nedergaard, J., May 5 2000. Norepinephrine induces vascular endothelial growth factor gene expression in brown adipocytes through a beta -adrenoreceptor/cAMP/protein kinase A pathway involving Src but independently of Erk1/2. Journal of Biological Chemistry 275:13802–13811.

